Excitons in one-dimensional van der Waals materials: Sb_2S_3 nanoribbons

Fabio Caruso, Marina R. Filip, and Feliciano Giustino
Department of Materials, University of Oxford, Parks Road, Oxford OX1 3PH, United Kingdom
(Received 12 July 2015; revised manuscript received 20 August 2015; published 17 September 2015)

Antimony sulphide Sb_2S_3 has emerged as a promising material for a variety of energy applications ranging from solar cells to thermoelectrics and solid-state batteries. The most distinctive feature of Sb_2S_3 is its crystal structure, which consists of parallel 1-nm-wide ribbons held together by weak van der Waals forces. This structure clearly suggests that it should be possible to isolate individual Sb_2S_3 ribbons using micromechanical or liquid-phase exfoliation techniques. However, it is not clear yet how to identify the ribbons postexfoliation using standard optical probes. Using state-of-the-art first-principles calculations based on many-body perturbation theory, here we show that individual ribbons of Sb_2S_3 carry optical signatures clearly distinct from those of bulk Sb_2S_3. In particular, we find a large blueshift of the optical absorption edge (from 1.38 to 2.30 eV) resulting from the interplay between a reduced screening and the formation of bound excitons. In addition, we observe a transition from an indirect band gap to a direct gap, suggesting an enhanced photoluminescence in the green. These unique fingerprints will enable extending the research on van der Waals materials to the case of one-dimensional chalchogenides.

DOI: 10.1103/PhysRevB.92.125134 PACS number(s): 71.20.−b, 74.70.Xa, 78.20.−e

I. INTRODUCTION

The development of micromechanical as well as liquid-phase exfoliation techniques [1–3] has triggered a surge of interest into two-dimensional (2D) materials and their uses in electronics, optics, and energy generation and storage [4–10]. Most current research focuses on the synthesis and manipulation of so-called "van der Waals" materials, that is, compounds with a layered structure where 2D sheets are held together by weak van der Waals interactions [6,11], and can be exfoliated into individual monolayers. 2D materials in this category include graphene [3], the transition metal dichalcogenide series [12], hexagonal boron nitride [13,14], and phosphorene [4,15,16].

Given the current momentum of research on 2D compounds, it is natural to ask whether some of these concepts could be extended to the case of one-dimensional (1D) van der Waals materials. A potential class of materials of this kind is provided by the minerals of the tetradymite family, namely, stibnite (Sb_2S_3), antimonselite (Sb_2Se_3), bismuthinite (Bi_2S_3), and guanajuatite (Bi_2Se_3). In fact, crystals of these compounds consist of ribbonlike structures featuring covalent metal-chalcogen bonds within each ribbon, and van der Waals bonds in between adjacent ribbons, as shown in Fig. 1 [17,18].

Among these compounds the mineral stibnite is widely available and constitutes a common additive to solid-state lubricants, such as graphite and molybdenite. Owing to its strong optical absorption in the visible range [19–22], Sb_2S_3 has successfully been employed as a semiconductor sensitizer in nanostructured solar cells [23–28], with the best devices reaching solar energy conversion efficiencies as high as 7.5% [24]. In addition, Sb_2S_3 can be intercalated as in the case of 2D chalcogenides, and has been used as a fast ion conductor in sodium-ion batteries [29]. Owing to its peculiar structure, it should be possible to exfoliate Sb_2S_3 into individual atomic ribbons ("nanoribbons" henceforth); indeed rods of transverse size ∼2 nm and length $>1\mu$m were synthesized via solution processing and imaged by Scanning Transmission Electron Microscopy in Ref. [30].

The availability of nanoribbons of Sb_2S_3 and more generally materials of the tetradymite family may open new avenues in research on 1D semiconductors with novel electronic and optical properties. In this context, it is important to establish the spectroscopic signatures of such structures to facilitate their identification and manipulation in experiments.

Here we investigate the optical properties of Sb_2S_3 in its bulk and nanoribbon forms from first principles. Using state-of-the-art many-body perturbation theory techniques based on the GW approximation and the Bethe-Salpeter equation we show that the electronic and optical properties of Sb_2S_3 are dramatically altered by dimensionality. In fact, Sb_2S_3 nanoribbons are found to be direct wide-gap semiconductors, in stark contrast to bulk stibnite which is an indirect visible-gap semiconductor. In addition, the interaction between electrons and holes in 1D leads to the formation of bound excitons and a substantial modification of the optical absorption line shape. Due to these peculiar optical properties, Sb_2S_3 nanoribbons may find applications in nanoscale green light emitting devices.

II. METHODS

Ground-state density-functional theory/local-density approximation (DFT/LDA) calculations were performed using the QUANTUM ESPRESSO suite [31]. We used a plane-waves kinetic energy cutoff of 90 Ry and scalar-relativistic norm-conserving Troullier-Martins pseudopotentials [32], generated using the FHI98 code [33]. For Sb (S), $5s$ and $5p$ ($3s$ and $3p$) electrons were included in the valence. The Brillouin zone was sampled using a $4\times8\times4\,(1\times8\times1)$ Monkhorst-Pack grid for bulk Sb_2S_3(nanoribbon). In the case of bulk Sb_2S_3 we used the experimental lattice parameters and atomic positions [17,34], whereas for the nanoribbon we used the optimized geometry in a supercell with transverse area of 50×50 Å^2. Quasiparticle GW calculations and the calculations of the optical spectra were performed using the YAMBO code [35]. The quasiparticle energies were computed in the G_0W_0 approximation [36]. The energy dependence of the GW self-energy was described by means of the Godby-Needs plasmon-pole model [37]. We used a plane-waves kinetic energy cutoff of 15 Ry (4 Ry) for the exchange (correlation) part of the GW self-energy, and a $2\times6\times2\,(1\times8\times1)$

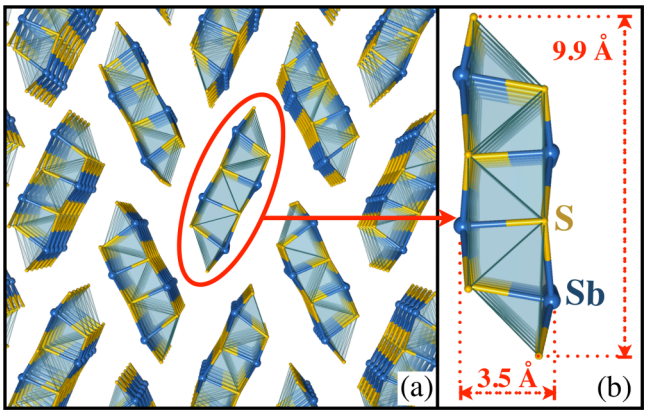

FIG. 1. (Color online) Ball-and-stick representations of (a) bulk Sb_2S_3 and a (b) 1D Sb_2S_3 nanoribbon. The Sb and S atoms are indicated in blue and yellow, respectively. The extent of the nanoribbon in the directions perpendicular to its axis is 9.9×3.5 Å^2.

Monkhorst-Pack grid for reciprocal-space integrals in the case of bulk (nanoribbon) Sb_2S_3. We used 270 bands in the sums over Kohn-Sham states, corresponding to unoccupied states up to 30 eV from the conduction band bottom. Convergence tests for all these parameters are reported in Ref. [38].

The optical absorption spectra were obtained by solving the Bethe-Salpeter equation in the electron-hole basis, within the Tamm-Dancoff approximation and using Haydock's recursion. We used DFT/LDA Kohn-Sham states for the electron-hole basis, and quasiparticle energies from G_0W_0 calculations. Brillouin-zone integrals were carried out using $4 \times 8 \times 4$ and $1 \times 8 \times 1$ points for bulk Sb_2S_3 and for the nanoribbon, respectively. The Bethe-Salpeter equation (BSE) kernel was described using a plane-waves kinetic energy cutoff of 3 Ry (4 Ry) for bulk (nanoribbon) Sb_2S_3. Calculations of the energy-loss function were performed using the RPA approximation and the GW quasiparticle band structure in the case of bulk Sb_2S_3. For the nanoribbon we performed an RPA calculation using the DFT/LDA bands, scissor-corrected using our calculated GW band gap (+1.83 eV). This simplification was necessary in order to make the calculations feasible (as the energy range of Fig. 4 involves >2000 electronic transitions).

III. QUASIPARTICLE AND OPTICAL PROPERTIES

Figure 1(a) shows a ball-and-stick model of bulk Sb_2S_3. This crystal structure was generated by using the experimental lattice parameters and the symmetry operations of the *Pnma* space group [17,34,38]. From this figure it is apparent that Sb_2S_3 consists of a collinear arrangement of one-dimensional $(Sb_4S_6)_n$ ribbons. The weak interribbon cohesive energy (0.2 eV/atom, to be compared to the intraribbon energy of 3.9 eV/atom) [38] and the negligible electron density in between adjacent ribbons [17] indicates that the three-dimensional structure of bulk Sb_2S_3 results from the van der Waals bonding of 1D nanoribbons. This suggests a close analogy with layered materials, such as graphite and transition-metal dichalcogenides, with the difference that in the present case the cleavage across the van der Waals gaps should result in 1D structures. Figure 1(b) shows a ball-and-stick model of an individual Sb_2S_3 nanoribbon cut out of bulk Sb_2S_3 and optimized using DFT [39,40] in the local-density approximation [41,42]. The optimized nanoribbon preserves all the structural parameters of bulk Sb_2S_3 (the largest deviation between bond lengths is 0.06 Å). In Fig. 5 in the Appendix, we show the calculated phonon dispersions of an individual Sb_2S_3 nanoribbon. The absence of soft modes indicates that individual nanoribbons are dynamically stable, supporting the notion that they should be amenable to exfoliation, similar to other layered chalcogenides. This observation is in line with previous molecular dynamics simulations of individual ribbons [43]. Additionally, it has recently been proposed that the electronic properties of Bi_2S_3 nanoribbons might be further modified by passivation of the nanoribbon surface with carboxylic and amine groups [44]. The same conclusion should hold also for Sb_2S_3 nanoribbons, owing to the similarity of their structure and stoichiometry to Bi_2S_3 nanoribbons.

Figure 2 shows the DFT/LDA band structure of bulk Sb_2S_3 and of an individual nanoribbon (all computational

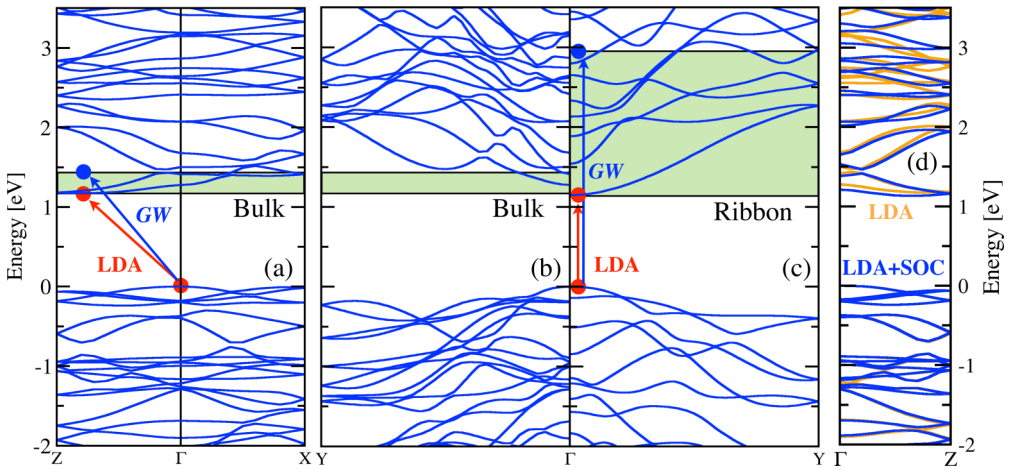

FIG. 2. (Color online) DFT/LDA band structures of (a), (b), (d) bulk Sb_2S_3 and of a (c) Sb_2S_3 nanoribbon. The shaded areas indicate the G_0W_0 quasiparticle corrections, and the arrows indicate the character of the fundamental gap (DFT/LDA in red, GW in blue). (d) shows the band structures of bulk Sb_2S_3 calculated with (blue) or without (orange) spin-orbit coupling.

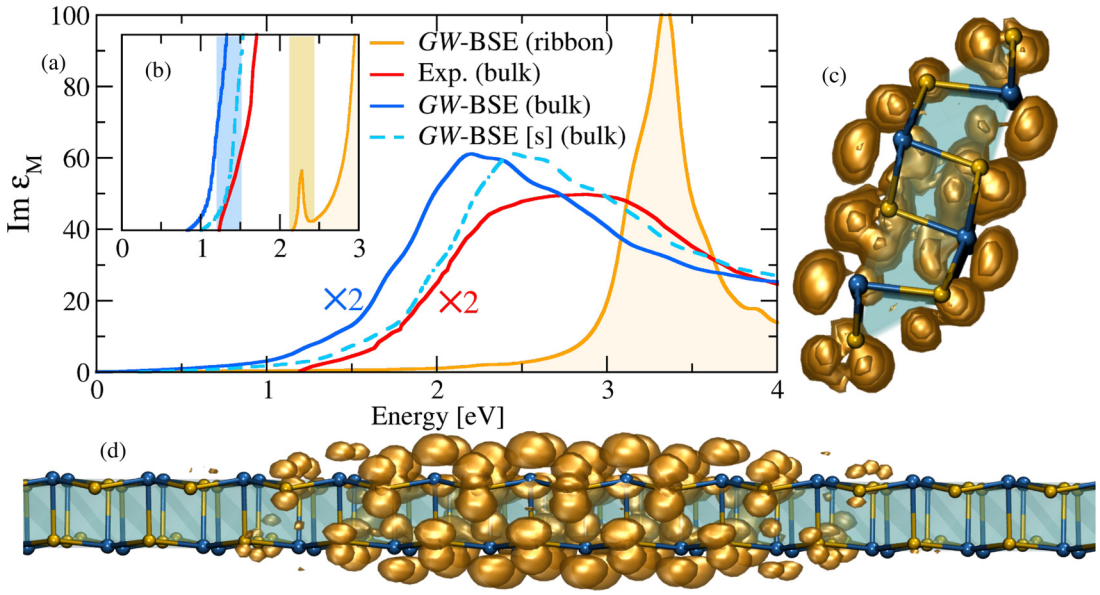

FIG. 3. (Color online) Optical absorption spectra of bulk Sb_2S_3 and Sb_2S_3 nanoribbon, and exciton wave function of Sb_2S_3 nanoribbon. (a) Comparison between the calculated imaginary part of the dielectric function of bulk Sb_2S_3(blue line) and individual nanoribbons (yellow line and shading), and the measured dielectric function (red line). The experimental data are from the generalized ellipsometry measurements of Ref. [51], with light polarized along the *b* axis (nanoribbon axis). The dashed line is a rigid shift by 0.25 eV of the *GW*-BSE calculations for the bulk. (b) Close-up near the absorption onset, indicating the onset values as shaded areas, as discussed in the text. (c), (d) Views of the lowest-energy exciton wave functions (square modulus) parallel and perpendicular to the Sb_2S_3 ribbon axis, respectively. For visualization purposes the hole is set to the center of the nanoribbon unit cell.

parameters are provided in the section on Methods). In the case of bulk Sb_2S_3 we find an indirect band gap of 1.17 eV between the top of the valence band at Γ and the bottom of the conduction band at *Z*, in agreement with previous theoretical [17,18,38,43,45–47] as well as experimental studies [19–22,48,49]. The inclusion of quasiparticle corrections in the *GW* approximation (shaded in Fig. 2) increases the gap to 1.41 eV while maintaining the indirect character of the fundamental gap, consistent with Ref. [38]. As illustrated in Fig. 2(a), the direct and indirect band gaps differ by ∼0.1 eV. In the case of the Sb_2S_3 nanoribbon the Brillouin zone is one-dimensional, and the wave vectors run along the Γ-*Y* direction of the bulk crystal. Accordingly, the conduction band bottom at the *Z* point of bulk Sb_2S_3 disappears, leaving a direct band gap at the Γ point [Figs. 2(b) and 2(c); we note that the Γ-*Z* direction is perpendicular to the nanoribbon axis]. The DFT/LDA band gap of the nanoribbon is 1.15 eV, very close to bulk Sb_2S_3. However the *GW* quasiparticle correction is significantly larger than in bulk, owing to the reduced dielectric screening in one dimension. As a result the quasiparticle band gap becomes as large as 2.97 eV. Our finding is consistent with the delta self-consistent field (ΔSCF) calculations of Ref. [50] for Bi_2S_3 nanoribbons of increasing length. Figure 2(d) shows that spin-orbit coupling does not affect the band structures appreciably; hence we will neglect this contribution in the following. In Ref. [44], it has been reported the occurrence of edge states in quadruple Bi_2S_3 nanoribbons slightly above the valence band top. Edge states are not present in the individual Sb_2S_3 nanoribbon, but we do not exclude their occurrence in larger aggregates of nanoribbons.

We now turn to the optical properties of bulk Sb_2S_3 and individual nanoribbons. The reduced dimensionality of the nanoribbon is expected to alter the optical properties of bulk Sb_2S_3 via two competing effects. On the one hand, the quasiparticle band gap of the nanoribbon is significantly blueshifted as a result of quantum confinement and more pronounced quasiparticle corrections than in bulk Sb_2S_3. On the other hand, the redshift of the optical band gap with respect to the quasiparticle gap is expected to be larger in the nanoribbon, since the electron-hole interaction is strengthened by the reduced dielectric screening and the spatial confinement of electron and hole within the same nanoribbon [52,53]. Intriguingly, both these effects decrease with the effective dielectric constant experienced by electrons and holes, and tend to cancel each other. In order to quantitatively describe the optical properties of the nanoribbon resulting from this competition, it is essential to employ a theory whereby electron-hole interactions are described entirely from first principles. To this aim we calculate the dielectric function of bulk Sb_2S_3 and individual nanoribbons using the BSE [54–57]. The BSE method constitutes the state-of-the-art in *ab initio* calculations of optical absorption spectra, and its accuracy has been proven for a variety of materials [58], including one-dimensional nanostructures [59]. We perform BSE calculations starting from the *GW* quasiparticle band structures described above, with the screened Coulomb interaction calculated within the random-phase approximation (RPA). All computational details are provided in the section on Methods.

Figure 3(a) shows a comparison between the optical absorption spectra of bulk Sb_2S_3 and an isolated nanoribbon, as obtained here from BSE calculations, as well as the measured optical absorption of bulk Sb_2S_3 [51]. Our calculations for bulk Sb_2S_3 are in excellent agreement with experiment: indeed we are able to closely reproduce the measured absorption onset,

line shape, and intensity. The small redshift of our spectrum with respect to experiment (0.2 eV) can be assigned to the underestimation of the GW band gap as compared to the experimental reference values. In fact, a rigid shift of the calculated spectrum by 0.25 eV [dashed lines in Figs. 3(a) and 3(b)] considerably reduces the discrepancy between the experimental and theoretical absorption spectrum. By fitting our calculated spectrum using standard expressions for the direct optical absorption edge [60] we determine an optical band gap of 1.38 ± 0.02 eV [Fig. 3(b)]. A comparison of this value with the quasiparticle band gap of 1.41 eV indicates that the exciton binding energy in bulk Sb_2S_3 is in the range 10–50 meV. This result is in line with the estimates made in Ref. [61] based on the Wannier exciton model, and indicates that at room temperature there should be essentially no bound excitons in bulk Sb_2S_3.

Having established the reliability of the BSE approach for studying optical absorption in bulk Sb_2S_3, we can now move to individual nanoribbons. Figure 3(a) shows that the absorption line shape of the nanoribbon is substantially different from that of bulk Sb_2S_3. In particular we recognize a sharp resonance around 3.3 eV, which is characteristic of one-dimensional systems [59]. This resonance corresponds to a blueshift and a narrowing of the absorption maximum which can be seen around 2.2 eV in the case of bulk Sb_2S_3 [blue line in Fig. 3(a)]. Figure 3(b) shows that the absorption onset of the nanoribbon is at 2.30 eV [small peak in Fig. 3(b)], indicating a significant blueshift with respect to bulk Sb_2S_3. Even more interestingly, by comparing the optical gap of 2.30 eV with the quasiparticle gap of 2.97 eV we find that the exciton binding energy in this case is as large as 0.7 eV. This value is one order of magnitude larger than in bulk Sb_2S_3, indicating (i) that strongly bound excitons should exist in the nanoribbon and (ii) they may provide evidence to unequivocally confirm the successful exfoliation of Sb_2S_3 nanoribbons. A similar finding was reported in the case of carbon nanotubes [59].

In order to rationalize the large exciton binding energy in Sb_2S_3 nanoribbons we show in Figs. 3(c) and 3(d) the wave function of the lowest-energy exciton, corresponding to the absorption onset at 2.30 eV. The exciton shown in Fig. 3 results from the combination of electron states from the conduction band bottom and hole states from the valence band top. The Sb-5p character of the conduction band and the S-3p character of the valence band are reflected in the lobes which are clearly visible in the wave function. At variance with bulk Sb_2S_3, where the exciton can lower its binding energy by mixing electronic states belonging to adjacent ribbons, in the case of the nanoribbon the exciton experiences a strong lateral confinement [Fig. 3(c)], leading to an increase of the Coulomb interaction strength. In addition we see in Fig. 3(d) that the exciton wave function extends over ~2 nm along the ribbon axis, indicating that this state lies at the boundary between Wannier excitons and Frenkel excitons. An estimate of the bare Coulomb interaction between the electron and the hole using the length of 2 nm as the average electron-hole separation gives 0.8 eV. This value is in line with the calculated binding energy, and provides a simple interpretation for the significant difference between excitons in bulk Sb_2S_3 and its nanoribbons.

The changes between the band gaps Sb_2S_3 nanoribbons and bulk may be attributed to the different spatial extent of the electronic states in these compounds. Whereas in the bulk the bonding orbitals may delocalize on different ribbons, in Sb_2S_3 nanoribbons the electron density is confined on a single ribbon. This affects the optical gap in two ways: on the one hand, the increase of exchange interaction leads to an opening of the band gap; on the other hand the reduction of electronic screening leads to a strong enhancement of electron-hole interaction which tends to reduce the optical band gap. The opening of the optical gap of Sb_2S_3 nanoribbons discussed above, thus, results from the competitions of these two effects, which act in an opposite way and tend to cancel each other. Similar conclusions should also apply to other compounds of the tetradymite family, such as Bi_2S_3 nanoribbons [62].

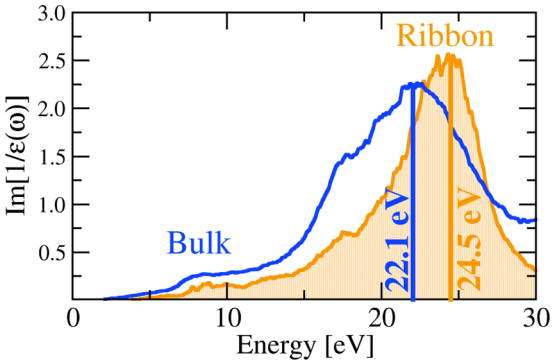

FIG. 4. (Color online) EELS spectrum (loss function) of bulk Sb_2S_3(blue line) and individual nanoribbons (yellow line) along the b axis (ribbon axis). The calculations are performed with the RPA using the quasiparticle band structure in the case of bulk Sb_2S_3, and the scissor-corrected DFT/LDA band structure in the case of the ribbon (see Methods).

Another significant difference between bulk Sb_2S_3 and individual nanoribbons can be found in their plasmonic properties. In fact, the blueshift of both the quasiparticle band gap and the optical gaps from three-dimensional Sb_2S_3 to 1D ribbons should be accompanied by a corresponding shift of the plasmon energies in these systems. This can be seen already in the simplest models of the frequency-dependent dielectric function of semiconductors, yielding [63] $E_p = [(\hbar\omega_p)^2 + E_g^2]^{1/2}$, where E_p is the energy of the plasmon, E_g the gap, and ω_p the plasma frequency of the valence electron density. Since the electron count (and hence the plasma frequency) is the same for the bulk and the nanoribbon, a change in the band gap must lead to a corresponding change in the plasmon energy. In order to test this hypothesis we calculated the energy-loss functions of bulk Sb_2S_3 and a ribbon along the b axis, within the RPA. Figure 4 shows that the energy loss spectrum of bulk Sb_2S_3 exhibits a shoulder at ~8.5 eV and a peak at ~22.1 eV. In the case of the Sb_2S_3 nanoribbon we find a qualitatively similar trend; however the low-energy shoulder and the high-energy peak appear at higher energies than in bulk Sb_2S_3. In particular the high-energy peak at ~24.5 eV is significantly blueshifted (by 2.4 eV) with respect to bulk Sb_2S_3. This blueshift constitutes another unique fingerprint of Sb_2S_3 nanoribbons, and could be used to identify these structures via electron-energy-loss spectroscopy (EELS) experiments on exfoliated stibnite samples.

IV. CONCLUSIONS

Taken together our results suggest at least three possible effects which can be used to identify Sb_2S_3 nanoribbons obtained by exfoliation of stibnite samples: (i) a strong blueshift (0.9 eV) of the optical absorption onset and a marked modification of the absorption line shape; (ii) a significant increase in the plasmon energy as measured by EELS (2.4 eV); (iii) a potential photoluminescence enhancement arising from the emergence of a direct band gap in the nanoribbon, which favors the radiative recombination of excitons. The latter effect is analogous to the case of MoS_2 [64], and should be observable near the absorption onset at 2.30 eV, that is, in the green region of the visible spectrum.

In summary, by means of state-of-the-art first-principles calculations we showed that Sb_2S_3 nanoribbons exhibit peculiar optical fingerprints which can be used not only to identify these nanostructures after bottom-up synthesis or exfoliation of the mineral stibnite, but also to develop novel one-dimensional light-emitting materials. More generally the unique strictly 1D structure of Sb_2S_3 ribbons as well as other nanoribbons of the tetradymite family (Sb_2Se_3 and Bi_2S_3) may open exciting new opportunities for studying Tomonaga-Luttinger physics [65], and should be accessible using exfoliation techniques established in the related area of two-dimensional materials [2,3].

ACKNOWLEDGMENTS

This work was supported by the Leverhulme Trust (Grant No. RL-2012-001) and the European Research Council (EU FP7 / ERC Grant No. 239578 and EU FP7/Grant No. 604391 Graphene Flagship). Calculations were performed at the Oxford Advanced Research Computing facility and at the Oxford Materials Modelling Laboratory.

APPENDIX: PHONON SPECTRUM OF Sb_2S_3 NANORIBBONS

In Fig. 5, we report the phonon spectrum of a single Sb2S3 nanoribbon for momenta along the Γ-Y direction. The phonon dispersion curves were calculated using density functional perturbation theory [66] as implemented in QUANTUM ESPRESSO. A $1 \times 14 \times 1$ Brillouin-zone grid was found to be sufficient for obtaining vibrational frequencies converged to within 10 cm^{-1}.

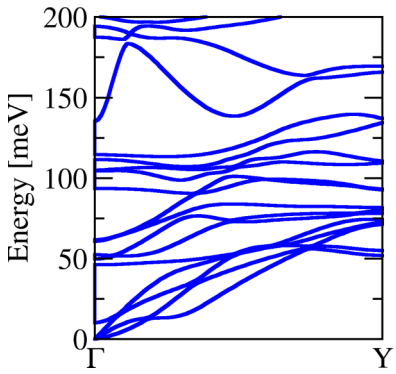

FIG. 5. (Color online) Calculated phonon dispersions of an Sb_2S_3 nanoribbon. There are no soft modes, indicating the dynamical stability of individual ribbons.

[1] J. N. Coleman *et al.*, Science **331**, 568 (2011).
[2] V. Nicolosi *et al.*, Science **340**, 6139 (2013).
[3] K. S. Novoselov *et al.*, Science **306**, 666 (2004).
[4] L. Li *et al.*, Nat. Nanotechnol. **9**, 372 (2014).
[5] B. Radisavljevic *et al.*, Nat. Nanotechnol. **6**, 147 (2011).
[6] A. K. Geim and I. V. Grigorieva, Nature (London) **499**, 419 (2013).
[7] F. Withers, O. Del Pozo-Zamudio, A. Mishchenko, A. P. Rooney, A. Gholinia, K. Watanabe, T. Taniguchi, S. J. Haigh, A. K. Geim, A. I. Tartakovskii, and K. S. Novoselov, Nat. Mater. **14**, 301 (2015).
[8] M.-L. Tsai *et al.*, ACS Nano **8**, 8317 (2014).
[9] F. Bonaccorso, Z. Sun, T. Hasan, and A. C. Ferrari, Nat. Photon. **4**, 611 (2010).
[10] Y. Zhu *et al.*, Science **332**, 1537 (2011).
[11] M. Chhowalla *et al.*, Nat. Chem. **5**, 263 (2013).
[12] Q. H. Wang *et al.*, Nat. Nanotechnol. **7**, 699 (2012).
[13] N. Alem, R. Erni, C. Kisielowski, M. D. Rossell, W. Gannett, and A. Zettl, Phys. Rev. B **80**, 155425 (2009).
[14] C. R. Dean *et al.*, Nat. Nanotechnol. **5**, 722 (2010).
[15] H. Liu, A. T. Neal, Z. Zhu, Z. Luo, X. Xu, D. Tomnek, and P. D. Ye, ACS Nano **8**, 4033 (2014).
[16] F. Xia, H. Wang, and Y. Jia, Nat. Commun. **5**, 4458 (2014).
[17] R. Caracas and X. Gonze, Phys. Chem. Miner. **32**, 295 (2005).
[18] C. E. Patrick and F. Giustino, Adv. Funct. Mater. **21**, 4663 (2011).
[19] R. H. Bube, J. Appl. Phys. **31**, 315 (1960).
[20] S. Mahanty, J. M. Merino, and M. Len, J. Vac. Sci. Technol. A **15**, 3060 (1997).
[21] J. Black *et al.*, J. Phys. Chem. Solids **2**, 240 (1957).
[22] I. K. El Zawawi, A. Abdel-Moez, F. S. Terra, and M. Mounir, Thin Solid Films **324**, 300 (1998).
[23] J. H. Rhee, C.-C. Chung, and E. W.-G. Diau, NPG Asia Mater. **5**, e68 (2013).
[24] Y. C. Choi, D. U. Lee, J. H. Noh, E. K. Kim, and S. I. Seok, Adv. Funct. Mater. **24**, 3587 (2014).
[25] G. Hodes, J. Phys. Chem. C **112**, 17778 (2008).
[26] G. Hodes and D. Cahen, Acc. Chem. Res. **45**, 705 (2012).
[27] S. Ito, K. Tsujimoto, D.-C. Nguyen, K. Manabe, and H. Nishino, Int. J. Hydrogen Energy **38**, 16749 (2013).
[28] D.-H. Kim, S.-J. Lee, M. S. Park, J.-K. Kang, J. H. Heo, S. H. Im, and S.-J. Sung, Nanoscale **6**, 14549 (2014).
[29] D. Y. W. Yu, P. V. Prikhodchenko, C. W. Mason, S. K. Batabyal, J. Gun, S. Sladkevich, A. G. Medvedev, and O. Lev, Nat. Commun. **4**, 2922 (2013).
[30] R. Malakooti, L. Cademartiri, A. Migliori, and G. A. Ozin, J. Mater. Chem. **18**, 66 (2008).
[31] P. Giannozzi *et al.*, J. Phys. Condens. Matter **21**, 395502 (2009).
[32] N. Troullier and J. L. Martins, Phys. Rev. B **43**, 1993 (1991).

[33] M. Fuchs and M. Scheffler, Comput. Phys. Commun. **119**, 67 (1999).
[34] P. Bayliss and W. Nowacki, Z. Kristallogr. **135**, 308 (1972).
[35] A. Marini *et al.*, Comput. Phys. Commun. **180**, 1392 (2009).
[36] M. S. Hybertsen and S. G. Louie, Phys. Rev. B **34**, 5390 (1986).
[37] R. W. Godby and R. J. Needs, Phys. Rev. Lett. **62**, 1169 (1989).
[38] M. R. Filip, C. E. Patrick, and F. Giustino, Phys. Rev. B **87**, 205125 (2013).
[39] P. Hohenberg and W. Kohn, Phys. Rev. **136**, B864 (1964).
[40] W. Kohn and L. J. Sham, Phys. Rev. **140**, A1133 (1965).
[41] J. P. Perdew and A. Zunger, Phys. Rev. B **23**, 5048 (1981).
[42] D. M. Ceperley and B. J. Alder, Phys. Rev. Lett. **45**, 566 (1980).
[43] R. Vadapoo *et al.*, Nanotechnol. **22**, 175705 (2011).
[44] V. Calzia, R. Piras, A. Ardu, A. Musinu, M. Saba, G. Bongiovanni, and A. Mattoni, J. Phys. Chem. C **119**, 16913 (2015).
[45] T. Ben Nasr *et al.*, Phys. B (Amsterdam, Neth.) **406**, 287 (2011).
[46] H. Koc *et al.*, Solid State Sci. **14**, 1211 (2012).
[47] J. J. Carey, J. P. Allen, D. O. Scanlon, and G. W. Watson, J. Solid State Chem. **213**, 116 (2014).
[48] M. Y. Versavel and J. A. Haber, Thin Solids Films **515**, 7171 (2007).
[49] N. Yesugade, C. Lokhande, and C. Bhosale, Thin Solids Films **263**, 145 (1995).
[50] V. Calzia, G. Molloci, G. Bongiovanni, and A. Mattoni, J. Phys. Chem. C **117**, 21923 (2013).
[51] M. Schubert *et al.*, Thin Solid Films **455-456**, 619 (2004).
[52] G. H. Wannier, Phys. Rev. **52**, 191 (1937).
[53] G. Dresselhaus, J. Phys. Chem. Sol. **1**, 14 (1956).
[54] L. Hedin, Phys. Rev. **139**, A796 (1965).
[55] G. Strinati, Riv. Nuovo Cimento **11**, 1 (1988).
[56] G. Onida, L. Reining, R. W. Godby, R. Del Sole, and W. Andreoni, Phys. Rev. Lett. **75**, 818 (1995).
[57] M. Rohlfing and S. G. Louie, Phys. Rev. B **62**, 4927 (2000).
[58] G. Onida, L. Reining, and A. Rubio, Rev. Mod. Phys. **74**, 601 (2002).
[59] C. D. Spataru, S. Ismail-Beigi, L. X. Benedict, and S. G. Louie, Phys. Rev. Lett. **92**, 077402 (2004).
[60] P. Yu and M. Cardona, in *Fundamentals of Semiconductors: Physics and Materials Properties*, Graduate Texts in Physics (Springer, Heidelberg, 2010).
[61] I. L. Validžić, M. Mitrić, N. D. Abazović, B. M. Jokić, A. S. Milošević, Z. S. Popović, and F. R. Vukajlović, Semicond. Sci. Technol. **29**, 035007 (2014).
[62] M. Aresti, M. Saba, R. Piras, D. Marongiu, G. Mula, F. Quochi, A. Mura, C. Cannas, M. Mureddu, A. Ardu, G. Ennas, V. Calzia, A. Mattoni, A. Musinu, and G. Bongiovanni, Adv. Funct. Mater. **24**, 3341 (2014).
[63] E. Tosatti and G. P. Parravicini, J. Phys. Chem. Solids **32**, 623 (1971).
[64] K. F. Mak, C. Lee, J. Hone, J. Shan, and T. F. Heinz, Phys. Rev. Lett. **105**, 136805 (2010).
[65] G. Mahan, in *Many-Particle Physics*, Physics of Solids and Liquids (Springer, Berlin, 2000).
[66] S. Baroni *et al.*, Rev. Mod. Phys. **73**, 515 (2001).